Bergische Universität Wuppertal

Fachbereich Mathematik und Naturwissenschaften

Institute of Mathematical Modelling, Analysis and Computational Mathematics (IMACM)

Preprint BUW-IMACM 16/29

Karsten Kahl, Nils Kintscher

Geometric Multigrid for the tight-binding Hamiltonian of graphene

November 4, 2016

GEOMETRIC MULTIGRID FOR THE TIGHT-BINDING HAMILTONIAN OF GRAPHENE

KARSTEN KAHL* AND NILS KINTSCHER*

Abstract. In order to calculate the electronic properties of graphene structures a tight-binding approach can be used. The tight-binding formulation leads to linear systems of equations which are maximally indefinite and can be seen both as a discretization of a system of PDEs or a staggered discretization. In this paper we develop a geometric multigrid method for this problem and undertake a complete two-level convergence analysis using local Fourier analysis. In numerical tests we show the scalability of the resulting multigrid method with respect to various geometric parameters.

Key words. geometric multigrid, indefinite operators, local Fourier analysis, staggered triangular grid, honeycomb lattice, tight-binding Hamiltonian, Graphene

AMS subject classifications. 65F10, 65N55, 65Z05

1. Introduction. In this paper we construct a well behaving geometric multigrid algorithm for a maximally indefinite (and for certain geometries even singular) linear system of equations. By using local Fourier analysis (LFA) we prove the convergence of the two-grid method.

The maximally indefinite system arises from the tight-binding approach for electronic structure calculations of graphene [10, 11, 19], which plays a key-role in computationally demanding simulations, such as Monte-Carlo studies [9, 22]. Herein, the indefinite operator is formulated on a honeycomb lattice which can be interpreted as a staggered triangular lattice.

Multigrid methods for indefinite problems have been considered mainly in the the context of the indefinite Helmholtz equation or other 2nd order elliptic boundary value problems. Typically, convergence of a multigrid method for these problems can only be guaranteed if particular conditions are fulfilled; cf. [1, 2, 5, 6, 20, 23]. The most prominent restriction oftentimes requires that the coarsest grid needs to be sufficiently fine/large. This means that there is no such method with the typical multigrid advantage—an asymptotic convergence rate independent of the grid size. Recently, in the context of Lattice Gauge Theory algebraic multigrid methods have experimentally been shown to be efficient for indefinite spin systems in [12, 16, 18]. However no theoretical proof of convergence is available for these methods.

LFA was introduced in [7, 8] and is known as a powerful tool for the convergence analysis of multigrid methods. A comprehensive introduction to LFA on rectangular grids can be found in [21]. The concept has been further developed to other triangular and hexagonal grids in [13, 24] and to systems of PDEs, e.g. curl-curl and Navier-Stokes, in [4, 17, 21]. In the LFA for the curl-curl equation, the PDE is discretized by first order edge elements on a regular quadrilateral grid such that the unknowns correspond to the edges of the grid. Since the edges in vertical direction are different from the edges in horizontal direction, the system and the LFA is treated as a staggered rectangular lattice which is very similar to the case discussed in here.

The remainder of this paper is organized as follows. First, we give an introduction about the geometric structure of graphene and the geometry of the graphene patches

*School of Mathematics and Natural Sciences, University of Wuppertal, 42097 Germany (kkahl@math.uni-wuppertal.de, kintscher@math.uni-wuppertal.de).

Funding: This work was partially funded by Deutsche Forschungsgemeinschaft (DFG) Transregional Collaborative Research Centre 55 (SFB/TRR55)

which are considered in this paper. Then we introduce the tight-binding Hamiltonian of graphene in its most general form and show how the spectrum of this operator can be extracted analytically. Afterwards, we sketch roughly the concept of multigrid methods and explain our construction in detail. At this point, the previously obtained spectral information of the operator is of crucial importance. The LFA which proves the convergence for the complete two-grid method is given right after. In the last section, numerical results are presented and compared to the results of the LFA. These results show the scalability of the twogrid and multigrid method with respect to several geometric parameters.

2. Graphene. Carbon materials occur in many different allotropes. Besides the well-known forms of graphite and diamond, reseachers recently isolated graphene, a single layer of carbon atoms bonded in a hexagonal or "honeycomb" structure. The distance a of two neighboring carbon atoms in graphene is approximately $1.42\mathring{A}$. Graphene is the basic element of fullerenes, which are molecules of carbons in the form of a sphere (Buckminsterfullerene C_{60}), tubes (carbon nanotubes) and many other shapes [10, 14]. In this paper we restrict ourselves to rectangular graphene sheets with different boundary conditions, which means we are dealing with sheets, tubes and tori. In order to describe these geometries in more detail, we first introduce notation for lattice structures and show how the hexagonal structure of graphene can be viewed as a triangular lattice with two atoms per lattice site.

Definition 1. *A 2-dimensional* lattice *generated by the vectors $a_1, a_2 \in \mathbb{R}^2$ is given by*

$$\mathbb{L} := \{x \in \mathbb{R}^2 \mid x = z_1 a_1 + z_2 a_2, \quad z_1, z_2 \in \mathbb{Z}\}.$$

While the hexagonal structure of graphene is not a lattice per se it can be interpreted as a triangular lattice $\mathbb{L}_T$ of pairs of atoms generated by the vectors

$$a_1 = (\frac{3a}{2}, \frac{\sqrt{3}a}{2}), \quad a_2 = (\frac{3a}{2}, -\frac{\sqrt{3}a}{2}) \tag{1}$$

as illustrated in Figure 1. The graphene lattice is then given by the set of points

$$\mathbb{L}_G := \{x + \delta\tau,\ x \in \mathbb{L}_T, \delta \in \{0,1\}\} \tag{2}$$

with $\tau := (a, 0)$. To distinguish the points we denote $x \in \mathbb{L}_T$ by type A and $x \in \mathbb{L}_G \backslash \mathbb{L}_T$ by type B.

Definition 2. *Define a rectangular graphene patch $\mathbb{G}_{n,m,\ell}$ with $n, m, \ell \in \mathbb{N}$ by*

$$\mathbb{G}_{n,m,\ell} := \mathbb{L}_G \cap R,$$

where $R := \{x \in \mathbb{R}^2 : x = \alpha_1 C + \alpha_2 T,\ \alpha_i \in (0,1]\}$. In here the boundary vectors of the confining rectangle R are given by

$$C = na_1 + ma_2 \quad \text{and} \quad T = \ell \left(\frac{2m+n}{N_r} a_1 - \frac{2n+m}{N_r} a_2 \right),$$

where $N_r = \gcd(2n{+}m, 2m{+}n)$[1]*. Its chiral angle is given by $\theta = -\frac{\pi}{6} + \tan^{-1}(\frac{\sqrt{3}m}{m+2n})$. One easily checks that T is indeed orthogonal to C; cf. Figure 2.*

[1] $\gcd(a, b)$ is the greatest common divisor of $a, b \in \mathbb{N}$

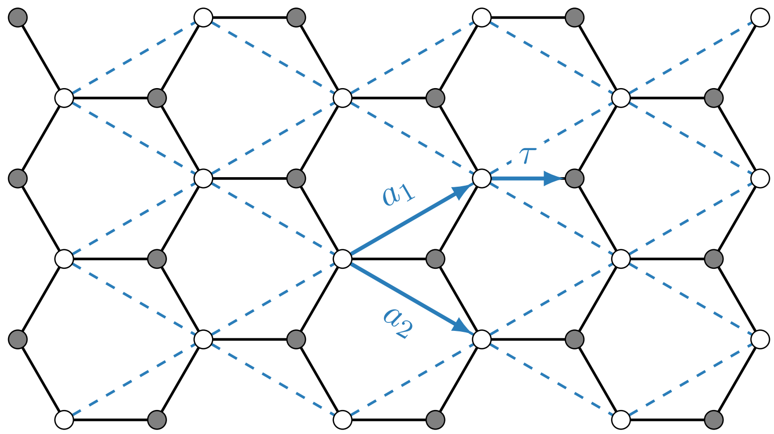

Figure 1: graphene interpreted as a triangular lattice $\mathbb{L}_T$ (○ A, ● B).

Remark 3. *Due to symmetries of the graphene lattice all possible rectangular patches* $\mathbb{G}_{n,m,\ell}$ *are defined by*

$$n, m, \ell \in \mathbb{N} \setminus 0 \quad \textit{and} \quad n \geq m,$$

which restricts the chiral angle to $0° \leq \theta < 30°$.

- *For* $n = m$ $(\theta = 0°)$*, we obtain an* armchair *boundary in the direction of* C *and a* zigzag *boundary in the direction of* T*, as illustrated by the horizontal and vertical boundary in Figure 2.*
- *The number of atoms in* $\mathbb{G}_{n,m,\ell}$ *is (cf. [11])*

$$|\mathbb{G}_{n,m,\ell}| = 2\frac{|C \times T|}{|a_1 \times a_2|} = \frac{4\ell(n^2 + nm + m^2)}{N_r}\,, \tag{3}$$

  where $\times$ *denotes the vector product operator.*

Carbon nanotubes are obtained from $\mathbb{G}_{n,m,\ell}$ by rolling it up along C such that $x \in \mathbb{G}_{n,m,\ell}$ is identified with $x + C$; cf. Figure 3.

Tight-binding Hamiltonian. In order to calculate the electronic band structure of graphene a tight-binding Hamiltonian approach is used which considers electrons hopping between lattice points with a hopping energy that decreases exponentially with distance. Due to the exponential decay of the hopping energy good approximations are already achieved by considering only couplings to the nearest, next-nearest and next-to-next nearest neighbors. To fix the notation for such an operator we use the concept of level sets.

Definition 4. *Let* $X = \{1, 2, \dots\}$ *denote all lattice sites and* $x_i \in \mathbb{R}^2$ *the coordinate of the ith lattice site. Then* level sets $G^i_j \neq \emptyset$ *with respect to lattice site* i *are defined by*

(i) $x, y \in G^i_j \Longrightarrow \|x_i - x\|_2 = \|x_i - y\|_2$

(ii) $j < k \Longleftrightarrow \|x_i - y\|_2 < \|x_i - z\|_2, \quad$ *for all* $y \in G^i_j, z \in G^i_k$.

In Figure 4 the level sets G^i_0, G^i_1, G^i_2 and G^i_3 are shown on the hexagonal structure. With the definition of level sets in place, the tight-binding Hamiltonian operator with

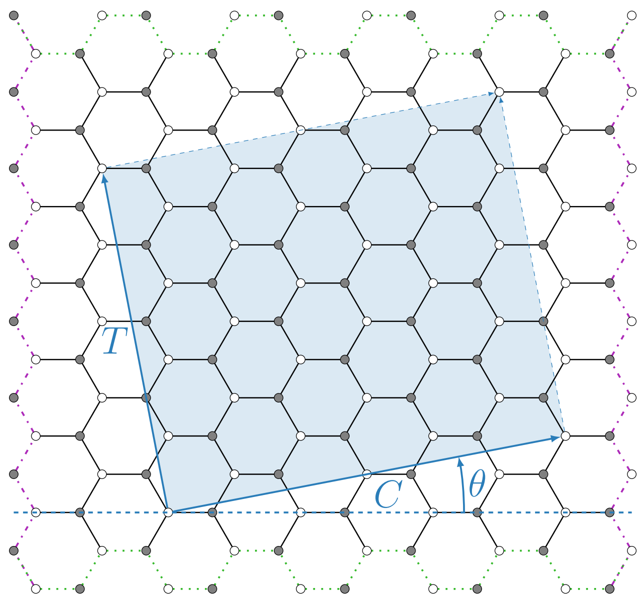

Figure 2: $G_{4,2,1}$, zigzag armchair boundary

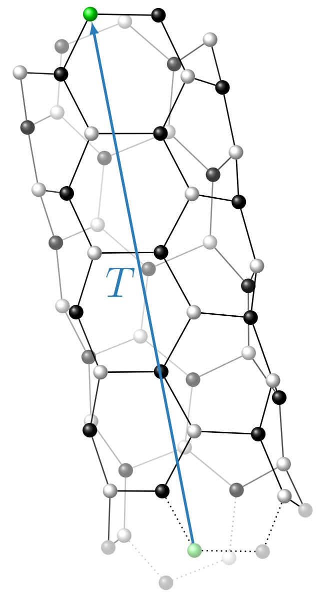

Figure 3: Nanotube $G_{4,2,1}$

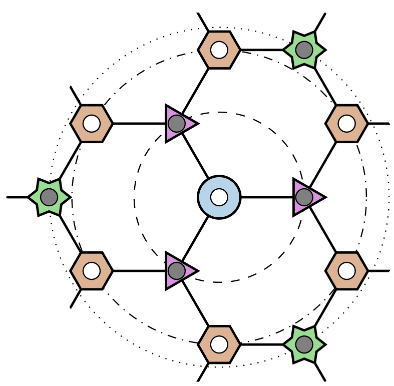

Figure 4: The first four level sets G_0, G_1, G_2 and G_3

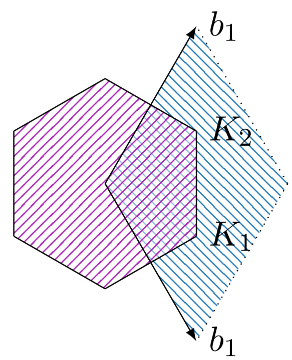

Figure 5: 1[st] Brillouin zone, $\mathbb{D}_G$

hopping energies $t_0, t_1, \ldots, t_M$ is defined by

$$(4) \qquad (A_{[t_0,t_1,t_2,\ldots,t_M]}x)_i = \sum_{j=0}^{M} t_j \sum_{\ell \in G_j^i} x_\ell, \quad \text{for all } i \in X.$$

Values $[t_0, t_1, \ldots]$ for the hopping energies found in the literature [19] are approximately $[0, -2.7, 0, 0, \ldots]eV$ ($[-.36, -2.78, -.12, -.068]eV$) in the nearest neighbor (third nearest neighbor) description.

Spectral properties. In the spectral analysis of operators on lattices the reciprocal lattice plays an important role. It has a direct relation to the Fourier transform on the lattice.

Definition 5. *Let $\mathbb{L}$ be a 2-dimensional lattice generated by the vectors a_1 and a_2. Then its* reciprocal *lattice is defined by vectors b_1 and b_2 such that*

$$\langle b_i, a_j \rangle_2 = 2\pi \cdot \delta_{ij}.$$

The reciprocal lattice of $\mathbb{L}_T$ is defined by the basis vectors

$$b_1 = \frac{2\pi}{3a}\left(1, \sqrt{3}\right), \quad b_2 = \frac{2\pi}{3a}\left(1, -\sqrt{3}\right).$$

For a local Fourier analysis it is sufficient to consider a finite area of the reciprocal lattice due to the periodicity of the Fourier modes, i.e.,

$$e^{i\langle k_1 b_1 + k_2 b_2, x\rangle_2} = 1, \quad k_1, k_2 \in \mathbb{Z}^2, x \in \mathbb{L}_T.$$

For example the paralellogram $\mathbb{D}_G$ spanned by the vectors b_1 and b_2, i.e.,

$$\mathbb{D}_G = \{k_1 b_1 + k_2 b_2, 0 \leq k_1, k_2 < 1\}.$$

In the context of solid state physics, it is more common to consider the *first Brillouin zone*, also known as the Wigner-Seitz cell or Voronoi cell of the reciprocal lattice, illustrated in Figure 5.

The spectrum of a locally defined operator on an infinite lattice can be computed using Bloch's theorem [3], which states that the eigenfunctions of an operator defined on a lattice are given by

$$\Psi(k, x) = e^{i\langle k, x\rangle_2} u(x),$$

where $k = k_1 b_1 + k_2 b_2, 0 \leq k_1, k_2 < 1$, $x \in \mathbb{L}$ and $u(x)$ is periodic on $\mathbb{L}$, i.e., $u(x + z_1 a_1 + z_2 a_2) = u(x), z_1, z_2 \in \mathbb{Z}$. With respect to the tight binding Hamiltonian of graphene we thus find the following description of its spectrum on an infinite lattice (shown in Figure 6).

Theorem 6. *The eigenvalues of $A_{[0,t_1]}$ are given by*

$$E(k) = \pm t_1 \sqrt{3 + 2\cos(\langle k, a_1\rangle_2) + 2\cos(\langle k, a_2\rangle_2) + 2\cos(\langle k, a_2 - a_1\rangle_2)}, \tag{5}$$

with corresponding eigenfunctions

$$\widehat{\Psi}(k, x) = \alpha_k^{(1)} \begin{pmatrix} \Psi(k, x) \\ \Psi(k, x+\tau) \end{pmatrix} + \alpha_k^{(2)} \begin{pmatrix} \Psi(k, x) \\ -\Psi(k, x+\tau) \end{pmatrix},$$

where $\Psi(k, x) = e^{i\langle k, x\rangle_2}$, $k \in \mathbb{D}_G$ and $x \in \mathbb{L}_T$.

Proof. We have

$$\begin{aligned} A_{[0,t_1]} \begin{pmatrix} \Psi(k, x) \\ \pm\Psi(k, x+\tau) \end{pmatrix} &= t_1 \begin{pmatrix} \Psi(k, x+\tau) + \Psi(k, x - a_1 + \tau) + \Psi(k, x - a_2 + \tau) \\ \pm\left[\Psi(k, x) + \Psi(k, x + a_1) + \Psi(k, x + a_2)\right] \end{pmatrix} \\ &= t_1 \begin{pmatrix} (1 + e^{-i\langle k, a_1\rangle_2} + e^{-i\langle k, a_2\rangle_2})\Psi(k, x+\tau) \\ \pm(1 + e^{i\langle k, a_1\rangle_2} + e^{i\langle k, a_2\rangle_2})\Psi(k, x) \end{pmatrix}. \end{aligned}$$

Thus we obtain the eigenvalues of the tight-binding Hamiltonian by diagonalizing the hermitian 2×2 matrix

$$\begin{pmatrix} 0 & 1 + e^{i\langle k, a_1\rangle_2} + e^{i\langle k, a_2\rangle_2} \\ 1 + e^{-i\langle k, a_1\rangle_2} + e^{-i\langle k, a_2\rangle_2} & 0 \end{pmatrix}. \tag{6}$$

□

Remark 7. *The zeroes of $E(k)$ from (5) are called* Dirac points *[10]. The two Dirac points in $\mathbb{D}_G$ are given by*

$$K_1 = \frac{1}{3}b_1 + \frac{2}{3}b_2 \quad \text{and} \quad K_2 = \frac{2}{3}b_1 + \frac{1}{3}b_2,$$

which can easily be checked by analyzing the real and imaginary part of the entries in (6) seperately.

A corresponding basis of the kernel is then given by

$$(7) \quad \begin{pmatrix} e^{i\langle K_1,x\rangle_2} \\ e^{i\langle K_1,x+\tau\rangle_2} \end{pmatrix}, \begin{pmatrix} e^{i\langle K_1,x\rangle_2} \\ -e^{i\langle K_1,x+\tau\rangle_2} \end{pmatrix}, \begin{pmatrix} e^{i\langle K_2,x\rangle_2} \\ e^{i\langle K_2,x+\tau\rangle_2} \end{pmatrix} \text{ and } \begin{pmatrix} e^{i\langle K_2,x\rangle_2} \\ -e^{i\langle K_2,x+\tau\rangle_2} \end{pmatrix}, x \in \mathbb{L}_T.$$

Note, that the points $K_i - \delta(b_j + \gamma b_i)$, $i,j = 1,2$, $\delta,\gamma = 0,1$ are the six vertices of the first Brillouin zone as illustrated in Figure 5.

The remainder of the paper deals with the treatment of the tight-binding Hamiltonian on finite sections of the graphene lattice. Typical boundary conditions for the rectangular graphene sheets $\mathbb{G}_{n,m,\ell}$ are *open* and *periodic*. Open boundary conditions are realized by simply omitting the terms of the operator which would belong to off-lattice points in (4). Periodic boundary conditions are defined by translation equalities of the kind

$$(8) \qquad x + C = x \text{ and } x + T = x \text{ for all } x \in \mathbb{G}_{n,m,\ell}.$$

Lemma 8. *The eigenvalues of the tight-binding Hamiltonian $A_{[0,t_1]}$ on a periodic rectangular graphene sheet $\mathbb{G}_{n,m,\ell}$ are given by*

$$E(k) = \pm t_1\sqrt{3 + 2\cos(\langle k,a_1\rangle_2) + 2\cos(\langle k,a_2\rangle_2) + 2\cos(\langle k,a_2 - a_1\rangle_2)},$$

where k is restricted to the discrete set $\Lambda_{n,m,\ell} \cap \mathbb{D}_G$ with

$$\Lambda_{n,m,\ell} := \left\{ \frac{1}{2(n^2+nm+m^2)}(z_1\widehat{a}_1 + z_2\widehat{a}_2), \quad z_1, z_2 \in \mathbb{Z} \right\}$$

where the basis vectors are given by

$$\widehat{a}_1 = \frac{n \cdot N_r}{\ell}b_1 - \frac{m \cdot N_r}{\ell}b_2 \quad \text{and} \quad \widehat{a}_2 = (2m+n)b_1 + (2n+m)b_2.$$

Thus $K_1, K_2 \in \Lambda_{n,m,\ell}$ iff

$$(n-m) \mod 3 = 0, \quad \ell \cdot m \mod N_r = 0, \quad \ell \cdot n \mod N_r = 0.$$

Proof. Using the identity translations (8) one can show that the eigenfunctions with $k \in \Lambda_{n,m,\ell}$ are well defined. Further, due to $|\mathbb{G}_{n,m,\ell}| = 2|\Lambda_{m,n,\ell} \cap \mathbb{D}_G|$ (cf. (3)) there cannot be any other eigenfunctions. The statement about the Dirac points K_1, K_2 is a direct consequence. ∎

Remark 9. *Both Theorem 6 and Lemma 8 can be generalized to arbitrary tight-binding Hamiltonians $A_{[t_0,t_1,t_2,\dots,t_M]}$. Using the specified lattice Fourier modes the operator is again block diagonalized into 2×2 blocks.*

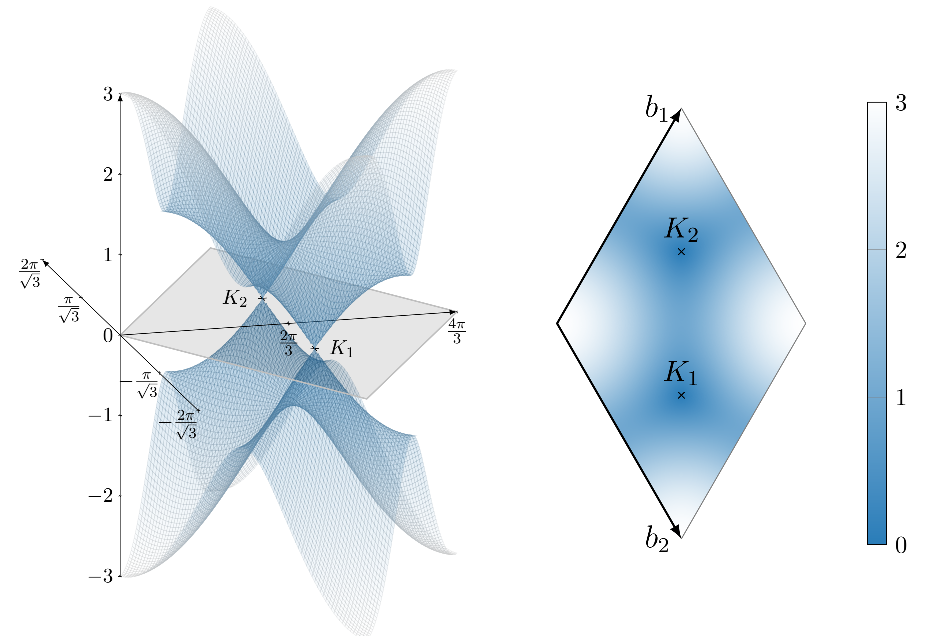

Figure 6: Spectrum of $A_{[0,-1]}$, i.e., $E(k), k \in \mathbb{D}_G$

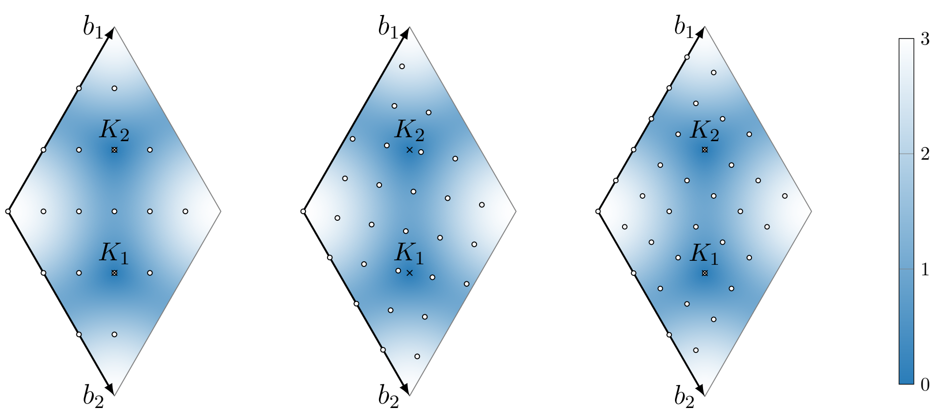

Figure 7: Discrete spectrum $\Lambda_{n,m,\ell}$ of $A_{[0,-1]}$ for different choices of (n, m, ℓ). Left $(3, 3, 3)$, middle $(4, 2, 1)$, right $(6, 0, 3)$.

3. Multigrid. Multigrid methods are iterative solvers for linear systems of equations $Ax = b, A \in \mathbb{R}^{n\times n}$ that exploit the geometric structure of the problem, such that in contrast to other iterative methods a convergence rate independent of the mesh size can be achieved. A multigrid method relies on the efficient interplay between a *smoother*, S, which typically is a simple stationary iterative scheme, and a coarse grid correction that is able to treat error components untouched by the smoother on a coarser scale. In order to formulate the coarse grid correction one first has to specify suitable coarse degrees of freedom. Oftentimes this corresponds to a splitting of the lattice points $\mathbb{L}_G$ of the current level into variables which are used on the coarse grid as well, $\mathbb{L}_G^c$, and the remainder $\mathbb{L}_G^f$. Once the choice of coarse degrees of freedom has been made, appropriate *interpolation* and *restriction* operators need to be defined

$$P : \mathbb{R}^{n_c} \to \mathbb{R}^n \quad \text{and} \quad R : \mathbb{R}^n \to \mathbb{R}^{n_c},$$

where n_c denotes the number of coarse degrees of freedom, e.g., $n_c = |\mathbb{L}_G^c|$. The coarse grid correction is then defined by its error propagator

$$I - P\,(RAP)^{-1}\,RA,$$

assuming that RAP is non-singular. In case A is symmetric the restriction R is typically chosen as P^T, which results in a Galerkin coarse grid correction. In Algorithm 1 we give a pseudo-code of the resulting two grid method. The (V-cycle) multigrid method is obtained by replacing $(RAP)^{-1}$ by (a single iteration of) yet another two grid method [21]. Note, that for the recursive applicability of the two grid construction on the coarse grid problem RAP one has to make sure that key features of A are preserved.

In what follows we specify the multigrid components for the graphene tight-binding Hamiltonian in more detail before we analyze the convergence of the resulting method in section 4.

Algorithm 1 Tentative two grid method

```
Given an initial guess x^(0), r^(0) = b − Ax^(0)
for all m = 1, 2, ... do
    x^(m) = S^ν1(A, x^(m−1), b)          ▷ pre-smooth ν1 times
    r_c = P^H(b − Ax^(m))                ▷ coarsen the residual
    A_c x_c = r_c                        ▷ solve the coarse grid problem
    x^(m) = x^(m) + P x_c                ▷ interpolate and correct
    x^(m) = S^ν2(A, x^(m), b)            ▷ post-smooth ν2 times
end for
```

Smoother. The smoother for our multigrid method is the Kaczmarz iteration [15], which can be viewed as the Gauss-Seidel iteration on the normal equations $A^TAx = A^Tb$. Given a splitting of A^TA into its diagonal and triangular parts

$$A^TA = D + L + U, \tag{9}$$

the Kaczmarz iteration can be written as

$$x \leftarrow x + (D+L)^{-1}(A^T(b - Ax)).$$

Note that the Kaczmarz iteration depends on the ordering of the unknowns. In here we use a lexicographic ordering as depicted in Figure 8. That is, we assume that the lattice points are numbered from bottom to top and left to right.

Coarse lattice points. We choose the splitting of lattice points $\mathbb{L}_G = \mathbb{L}_G^c \cup \mathbb{L}_G^f$ into coarse and fine lattice points in a way that guarantees the recursive applicability of the coarse grid construction. That is, the set of coarse grid lattice points should again be a honeycomb lattice.

We achieve this by defining a coarse triangular lattice

$$\mathbb{L}_T^c := \{\tau + z_1 \cdot 2a_1 + z_2 \cdot 2a_2,\ z_1, z_2 \in \mathbb{Z}\}.$$

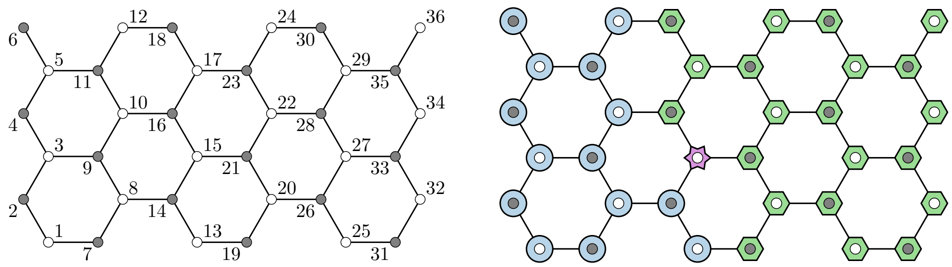

Figure 8: Lexicographic ordering of the graphene lattice (left) and status of unknowns within a Kaczmarz iteration (right). Unknowns already updated ◯; current unknown to be updated ✡; remaining unknowns not yet updated ⬡.

The corresponding coarse honeycomb lattice L_G^c is then given by

$$\mathbb{L}_G^c := \{x + \delta \cdot 2\tau,\ x \in \mathbb{L}_T^c,\ \delta \in \{0,1\}\}.$$

The coarse lattice points are identified by having a coarse lattice point located on the opposite site of any of the adjacent hexagons; cf. Figure 9. Using the same naming convention as in section 2 for the coarse lattice points, we denote $x \in \mathbb{L}_T^c$ by type A^c and $x \in \mathbb{L}_G^c \setminus \mathbb{L}_T^c$ by type B^c. Thus type A^c (B^c) lattice points are of type B (A) on the fine lattice.

Defining sublattices

$$\mathbb{L}_T^{(\zeta_1,\zeta_2)} := \{x + \zeta_1 a_1 + \zeta_2 a_2,\ x \in \mathbb{L}_T^c\}, \tag{10}$$

with $\mathbb{L}_T^{(0,0)} = \mathbb{L}_T^c$, the fine lattice can be split into

$$\mathbb{L}_T = \bigcup_{(\zeta_1,\zeta_2)\in\{0,1\}^2} \mathbb{L}_T^{(\zeta_1,\zeta_2)}.$$

Given this splitting of $\mathbb{L}_T$ one also obtains a splitting of $\mathbb{L}_G$ by

$$\mathbb{L}_G^{(\zeta_1,\zeta_2)} := \{x + \delta 2\tau,\ x \in \mathbb{L}_T^{(\zeta_1,\zeta_2)},\ \delta \in \{0,1\}\} \tag{11}$$

as illustrated in Figure 10.

Intergrid transfer. Due to the fact that the tight-binding Hamiltonian of graphene results in a symmetric linear operator we choose to use a Galerkin construction, i.e., $R = P^T$, and thus can restrict the discussion to the construction of P. Given a splitting of the lattice points $\mathbb{L}_G = \mathbb{L}_G^c \cup \mathbb{L}_G^f$, the main idea in the construction of the interpolation operator

$$P : \mathbb{L}_G^c \to \mathbb{L}_G, \quad P|_{\mathbb{L}_G^c} = I$$

is the exact preservation of kernel modes of the tight-binding Hamiltonian. That is, we want the interpolation operator to interpolate the Fourier modes (7) corresponding to the Dirac points K_1, K_2 exactly in the following sense

$$\begin{pmatrix} e^{i\langle K_j,x\rangle_2} \\ \pm e^{i\langle K_j,x+\tau\rangle_2} \end{pmatrix} = P \begin{pmatrix} \pm e^{i\langle K_j,y\rangle_2} \\ e^{i\langle K_j,y+2\tau\rangle_2} \end{pmatrix},\ j = 1,2,\ x \in \mathbb{L}_T,\ y \in \mathbb{L}_T^c. \tag{12}$$

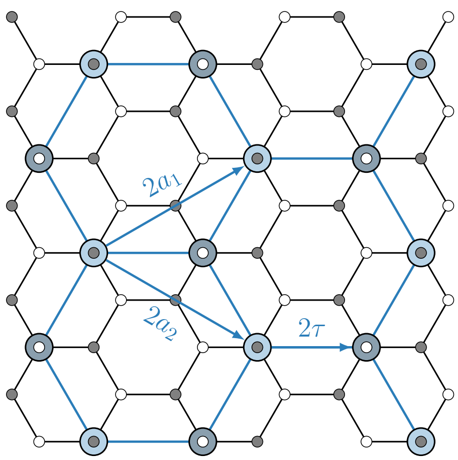

Figure 9: Coarse lattice $\mathbb{L}^c_G \subset \mathbb{L}_G$ and coarse lattice vectors of $\mathbb{L}^c_T$.

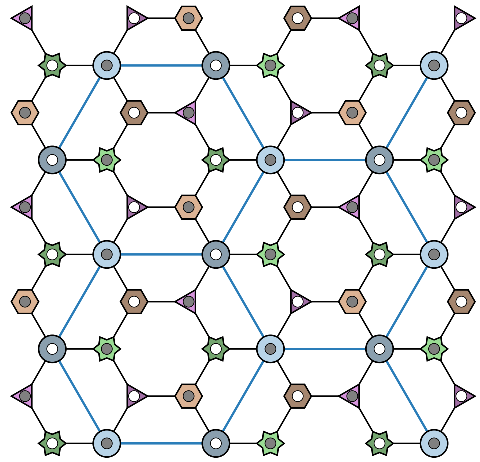

Figure 10: Splitting of $\mathbb{L}_G$ into / $L_G^{(0,0)}$, / $L_G^{(0,1)}$, / $L_G^{(1,0)}$ and / $L_G^{(1,1)}$.

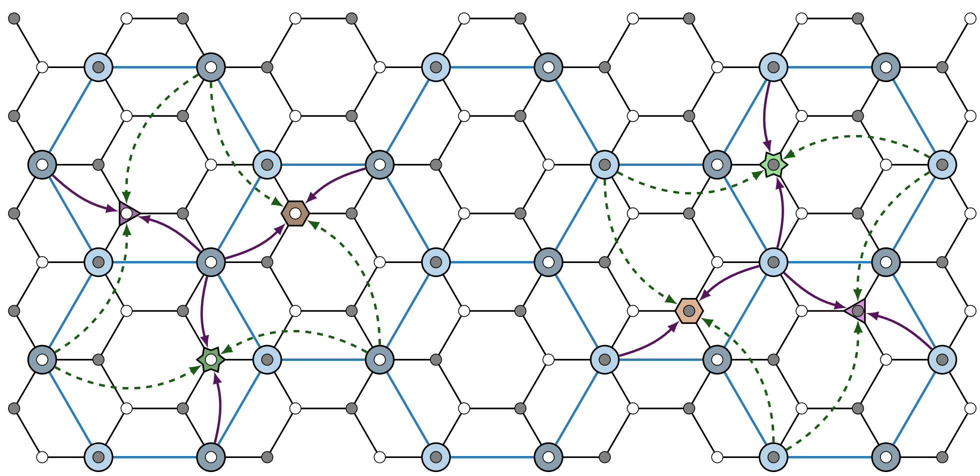

Figure 11: Illustration of interpolation using weights w_s and w_ℓ.

The problem of preserving these four modes can be reduced to a problem involving only two by choosing the interpolation points according to the species (either A or B) of the fine lattice point that is the target of interpolation. That is, a coarse lattice point of species A^c or B^c interpolates only to fine lattice points of species B or A, respectively. With this choice the $\pm$ term cancels, which halves the number of modes to fit and thus it only requires the solution of the interpolation problem (12) for either species A or B.

In addition the interpolation points should consist of coarse lattice points in the vicinity of the fine lattice point. Even though two interpolation points would be sufficient to resolve (12) we opt to define four interpolation points for each lattice point $x \in \mathbb{L}_G \setminus \mathbb{L}_G^c$ as illustrated in Figure 11.

Let $x \in \mathbb{L}_G^{(0,1)}$, then interpolation weights $w = (w_s, \widetilde{w}_s, w_\ell, \widetilde{w}_\ell)^T$ are obtained as solutions of the linear system of equations

$$\begin{pmatrix} e^{i\langle K_1, x+a_2\rangle_2} & e^{i\langle K_1, x-a_2\rangle_2} & e^{i\langle K_1, x+2a_1-a_2\rangle_2} & e^{i\langle K_1, x-2a_1+a_2\rangle_2} \\ e^{i\langle K_2, x+a_2\rangle_2} & e^{i\langle K_2, x-a_2\rangle_2} & e^{i\langle K_2, x+2a_1-a_2\rangle_2} & e^{i\langle K_2, x-2a_1+a_2\rangle_2} \end{pmatrix} w = \begin{pmatrix} e^{i\langle K_1, x\rangle_2} \\ e^{i\langle K_2, x\rangle_2} \end{pmatrix}$$

$$\Leftrightarrow \qquad \begin{pmatrix} e^{2\pi i 2/3} & e^{-2\pi 2/3} & e^{0\pi i} & e^{-0\pi i} \\ e^{2\pi i 1/3} & e^{-2\pi i 1/3} & e^{2\pi i} & e^{-2\pi i} \end{pmatrix} w = \begin{pmatrix} 1 \\ 1 \end{pmatrix}$$

$$\Leftrightarrow \qquad \begin{pmatrix} -\frac{1}{2} - \frac{\sqrt{3}}{2} i & -\frac{1}{2} + \frac{\sqrt{3}}{2} i & 1 & 1 \\ -\frac{1}{2} + \frac{\sqrt{3}}{2} i & -\frac{1}{2} - \frac{\sqrt{3}}{2} i & 1 & 1 \end{pmatrix} w = \begin{pmatrix} 1 \\ 1 \end{pmatrix} .$$

By choosing the interpolation weights to points symmetric to the fine lattice point to be equal, i.e., $\widetilde{w}_s = w_s$ and $\widetilde{w}_\ell = w_\ell$ the linear system of equations results in the relation

$$w_s = 2w_\ell - 1 . \tag{13}$$

Note, that due to symmetry this result is independent of the choice of

$$x \in \mathbb{L}_G^{(\zeta_1,\zeta_2)}, \ (\zeta_1, \zeta_2) \in \{0,1\}^2 \setminus (0,0).$$

We now analyze for which choices of pairs w_s, w_ℓ fulfilling (13) the multigrid method converges.

4. Theoretical Analysis. A commonly used tool in the analysis of multigrid methods on lattices, i.e., regularly structured discretizations which lead to stencil operators, is the local Fourier analysis (LFA) [21]. By neglecting boundary conditions, i.e., considering the operator on the infinite lattice

$$\mathbb{L}_G := \{x + \delta\tau : x \in \mathbb{L}_T, \delta \in \{0,1\}\},$$

LFA allows us to calculate upper bounds for the convergence rate of the two grid method. LFA uses the observation that the tight-binding Hamiltonian, which is described by a stencil on a lattice, is block-diagonalized by the Fourier modes

$$\begin{pmatrix} e^{i\langle k, x\rangle_2} \\ \pm e^{i\langle k, x+\tau\rangle_2} \end{pmatrix}, \quad k \in \mathbb{D}_G, x \in \mathbb{L}_T$$

(cf. section 2, in particular Theorem 6). For the sake of simplicity we limit ourselves in the analysis to the case $A = A_{[0,-1]}$. All results can be generalized to higher order tight-binding Hamiltonians $A_{[t_0,t_1,\ldots,t_M]}$ as well.

Two-grid analysis. In the LFA analysis of our two grid method we first provide a result for every component of the method, i.e., the operator A itself, the smoother S and the coarse grid correction. Then we conclude with an estimate of the asymptotic convergence rate defined by the 2-norm of the two grid error propagator

$$M = S\left(I - P\left(P^T A P\right)^{-1} P^T A\right) S.$$

DEFINITION 10. *Let $k = k_1 b_1 + k_2 b_2 \in \mathbb{D}_G$ with $k_1, k_2 \in [0, \frac{1}{2})$, then the eight-dimensional* space of harmonics *is defined by*

$$H_k = \{\varphi^{\pm}_{\xi_1,\xi_2}(k,x) := \begin{pmatrix} e^{i\langle k+\xi_1 \frac{b_1}{2} + \xi_2 \frac{b_2}{2}, x\rangle_2} \\ \pm e^{i\langle k+\xi_1 \frac{b_1}{2} + \xi_2 \frac{b_2}{2}, x+\tau\rangle_2} \end{pmatrix}, \ x \in \mathbb{L}_T, (\xi_1,\xi_2) \in \{0,1\}^2\}.$$

Any operator X which is H_k-invariant for all k can then be expressed by a family of 8×8 Matrices $X_k : H_k \to H_k$, defined by

$$XV_k = X_k V_k,$$

where $V_k = \begin{pmatrix}\varphi_{0,0}^{+} & \varphi_{0,0}^{-} & \varphi_{0,1}^{+} & \varphi_{0,1}^{-} & \varphi_{1,0}^{+} & \varphi_{1,0}^{-} & \varphi_{1,1}^{+} & \varphi_{1,1}^{-}\end{pmatrix}^T$ is the (ordered) collection of the 8 harmonic functions corresponding to k.

The amplification factor *of H at k is defined as $\rho(H_k) = \sqrt{\lambda_{\max}(H_k^T H_k)}$.*

We now show that M is an H_k-invariant operator and give a product formula for M_k. We start with the analysis of the tight-binding operator $A_{[0,-1]}$.

Lemma 11. *Let $k = k_1 b_1 + k_2 b_2 \in \mathbb{D}_G$ with $k_1, k_2 \in [0, \frac{1}{2})$ and $A = A_{[0,-1]}$, then A is H_k-invariant and A_k is a block-diagonal matrix with four blocks $A_{\widehat{k}} \in \mathbb{R}^{2\times 2}$, $\widehat{k} \in \{k + \xi_1 \frac{b_1}{2} + \xi_2 \frac{b_2}{2}, (\xi_1, \xi_2) \in \{0, 1\}^2\}$ with*

$$A_{\widehat{k}} = \begin{pmatrix} 0 & 1 + e^{i\langle \widehat{k}, a_1\rangle_2} + e^{i\langle \widehat{k}, a_2\rangle_2} \\ 1 + e^{-i\langle \widehat{k}, a_1\rangle_2} + e^{-i\langle \widehat{k}, a_2\rangle_2} & 0 \end{pmatrix}.$$

Proof. See Theorem 6. ∎

Lemma 12. *Let $k = k_1 b_1 + k_2 b_2 \in \mathbb{D}_G$ with $k_1, k_2 \in [0, \frac{1}{2})$, $A = A_{[0,-1]}$, then the Kaczmarz smoother given by its error propagator*

$$S = -(L + D)^{-1} U$$

based on the splitting (9) is H_k-invariant and, assuming lexicographic ordering, S_k is block-diagonal with four blocks $S_{\widehat{k}} \in \mathbb{R}^{2\times 2}$ corresponding to $\widehat{k} \in \{k + \xi_1 \frac{b_1}{2} + \xi_2 \frac{b_2}{2},\ (\xi_1, \xi_2) \in \{0, 1\}^2\}$. Each block $S_{\widehat{k}}$ fulfills

$$S_{\widehat{k}} = \begin{pmatrix} -\frac{e^{i\langle \widehat{k}, a_1\rangle_2} + e^{i\langle \widehat{k}, a_2\rangle_2} + e^{i\langle \widehat{k}, a_1 - a_2\rangle_2}}{3 + e^{i\langle \widehat{k}, -a_1\rangle_2} + e^{i\langle \widehat{k}, -a_2\rangle_2} + e^{i\langle \widehat{k}, -a_1 + a_2\rangle_2}} & 0 \\ 0 & -\frac{e^{i\langle \widehat{k}, a_1\rangle_2} + e^{i\langle \widehat{k}, a_2\rangle_2} + e^{i\langle \widehat{k}, a_1 - a_2\rangle_2}}{3 + e^{i\langle \widehat{k}, -a_1\rangle_2} + e^{i\langle \widehat{k}, -a_2\rangle_2} + e^{i\langle \widehat{k}, -a_1 + a_2\rangle_2}} \end{pmatrix}.$$

Proof. This statement is a direct consequence of $A^T A = A_{[3,0,1]}$. ∎

Concerning the coarse grid correction we first give an expression for the action of the restriction and interpolation. We introduce for each $k = k_1 b_1 + k_2 b_2 \in \mathbb{D}_G$ with $k_1, k_2 \in [0, \frac{1}{2})$ the space H_k^c by

$$H_k^c := \{\varphi_c^{\pm}(k, x) := \begin{pmatrix} \pm e^{i\langle k, x\rangle_2} \\ e^{i\langle k, x + 2\tau\rangle_2} \end{pmatrix},\ x \in \mathbb{L}_T^c\}.$$

Analogously to V_k we define $V_k^c = \begin{pmatrix}\varphi_c^{+} & \varphi_c^{-}\end{pmatrix}^T$.

Lemma 13. *Let $k = k_1 b_1 + k_2 b_2 \in \mathbb{D}_G$ with $k_1, k_2 \in [0, \frac{1}{2})$ the restriction operator P^T with interpolation weights w_s and w_ℓ maps $H_k \to H_k^c$. Thus it can be represented by $R_k \in \mathbb{C}^{2\times 8}$ such that $RV_k = V_k^c R_k$. The 2×2 blocks of R_k, corresponding to $\widehat{k} = k + (\xi_1 \frac{b_1}{2} + \xi_2 \frac{b_2}{2})$, $(\xi_1, \xi_2) \in \{0, 1\}^2$, are given by*

$$R_k^{(\xi_1,\xi_2)} = \frac{1}{2}\begin{pmatrix} \gamma_{\xi_1,\xi_2}(3\tau) + \gamma_{\xi_1,\xi_2}(\tau) & \gamma_{\xi_1,\xi_2}(3\tau) - \gamma_{\xi_1,\xi_2}(\tau) \\ \gamma_{\xi_1,\xi_2}(3\tau) - \gamma_{\xi_1,\xi_2}(\tau) & \gamma_{\xi_1,\xi_2}(3\tau) + \gamma_{\xi_1,\xi_2}(\tau) \end{pmatrix} \cdot \beta_{\widehat{k}}^{(0\,0\,0\,0)}, \tag{14}$$

where $\gamma_{\xi_1,\xi_2}(\mu) = e^{i\langle \xi_1 \frac{b_1}{2} + \xi_2 \frac{b_2}{2}, \mu\rangle_2}$ *and*

$$\begin{aligned} \beta_{\widehat{k}}^{(i_1\ i_2\ i_3\ i_4)} &= (-1)^{i_1} \cdot 1 \\ &+ (-1)^{i_2} \cdot 2[w_s \cos(\langle \widehat{k}, a_2\rangle_2) + w_\ell \cos(\langle \widehat{k}, 2a_1 - a_2\rangle_2)] \\ &+ (-1)^{i_3} \cdot 2[w_s \cos(\langle \widehat{k}, a_1\rangle_2) + w_\ell \cos(\langle \widehat{k}, a_1 - 2a_2\rangle_2)] \\ &+ (-1)^{i_4} \cdot 2[w_s \cos(\langle \widehat{k}, a_1 - a_2\rangle_2) + w_\ell \cos(\langle \widehat{k}, a_1 + a_2\rangle_2)]. \end{aligned} \tag{15}$$

Proof. Let $x_c = 2j_1 a_1 + 2j_2 a_2 + \tau \in \mathbb{L}_T^c$, i.e., of type A^c/B, then with $\beta_{\widehat{k}}^{(i_1\ i_2\ i_3\ i_4)}$ of (15) we find

$$\begin{aligned} R\begin{pmatrix} e^{i\langle \widehat{k}, x\rangle_2} \\ \pm e^{i\langle \widehat{k}, x+\tau\rangle_2} \end{pmatrix} &= \begin{pmatrix} \pm e^{i\langle \widehat{k}, x_c\rangle_2}(1 + w_s \cdot \sum\limits_{x_c + x_s \in G_2^{x_c}} e^{i\langle \widehat{k}, x_s\rangle_2} + w_\ell \cdot \sum\limits_{x_c + x_\ell \in G_5^{x_c}} e^{i\langle \widehat{k}, x_\ell\rangle_2}) \\ e^{i\langle \widehat{k}, x_c + 2\tau\rangle_2}(1 + w_s \cdot \sum\limits_{x_c + x_s + 2\tau \in G_2^{x_c+2\tau}} e^{i\langle \widehat{k}, x_s\rangle_2} + w_\ell \cdot \sum\limits_{x_c + x_\ell + 2\tau \in G_5^{x_c+2\tau}} e^{i\langle \widehat{k}, x_\ell\rangle_2}) \end{pmatrix} \\ &= \begin{pmatrix} \pm e^{i\langle \widehat{k}, x_c\rangle_2} \beta_{\widehat{k}}^{(0\,0\,0\,0)} \\ e^{i\langle \widehat{k}, x_c + 2\tau\rangle_2} \beta_{\widehat{k}}^{(0\,0\,0\,0)} \end{pmatrix} \\ &= \begin{pmatrix} \pm e^{i\langle k, x_c\rangle_2} e^{i\langle \xi_1 \frac{b_1}{2} + \xi_2 \frac{b_2}{2}, 2j_1 a_1 + 2j_2 a_2 + \tau\rangle_2} \beta_{\widehat{k}}^{(0\,0\,0\,0)} \\ e^{i\langle k, x_c + 2\tau\rangle_2} e^{i\langle \xi_1 \frac{b_1}{2} + \xi_2 \frac{b_2}{2}, 2j_1 a_1 + 2j_2 a_2 + 3\tau\rangle_2} \beta_{\widehat{k}}^{(0\,0\,0\,0)} \end{pmatrix} \\ &= \begin{pmatrix} \pm e^{i\langle k, x_c\rangle_2} \gamma_{\xi_1,\xi_2}(\tau) \beta_{\widehat{k}}^{(0\,0\,0\,0)} \\ e^{i\langle k, x_c + 2\tau\rangle_2} \gamma_{\xi_1,\xi_2}(3\tau) \beta_{\widehat{k}}^{(0\,0\,0\,0)} \end{pmatrix}. \end{aligned}$$

Solving the resulting 2×2 linear systems of equations yields (14). ∎

LEMMA 14. *Let* $k = k_1 b_1 + k_2 b_2 \in \mathbb{D}_G$ *with* $k_1, k_2 \in [0, \frac{1}{2})$. *The interpolation operator* P *with interpolation weights* w_s *and* w_ℓ *maps* $H_k^c \to H_k$. *Thus it can be represented by* $P_k \in \mathbb{C}^{8\times 2}$ *with* $PV_k^c = V_k P_k$. *Using again the notation of* (15) *we have*

$$P_k = \frac{1}{8}\begin{pmatrix} 2 \cdot \beta_k^{(0\,0\,0\,0)} & 0 \cdot \beta_k^{(0\,0\,0\,0)} \\ 0 \cdot \beta_k^{(0\,0\,0\,0)} & 2 \cdot \beta_k^{(0\,0\,0\,0)} \\ (1 - \gamma_{0,1}(-\tau))\beta_k^{(1\,0\,1\,0)} & (1 + \gamma_{0,1}(-\tau))\beta_k^{(1\,0\,1\,0)} \\ (1 + \gamma_{0,1}(-\tau))\beta_k^{(1\,0\,1\,0)} & (1 - \gamma_{0,1}(-\tau))\beta_k^{(1\,0\,1\,0)} \\ (1 - \gamma_{1,0}(-\tau))\beta_k^{(1\,1\,0\,0)} & (1 + \gamma_{1,0}(-\tau))\beta_k^{(1\,1\,0\,0)} \\ (1 + \gamma_{1,0}(-\tau))\beta_k^{(1\,1\,0\,0)} & (1 - \gamma_{1,0}(-\tau))\beta_k^{(1\,1\,0\,0)} \\ (1 + \gamma_{1,1}(-\tau))\beta_k^{(0\,1\,1\,0)} & (1 - \gamma_{1,1}(-\tau))\beta_k^{(0\,1\,1\,0)} \\ (1 - \gamma_{1,1}(-\tau))\beta_k^{(0\,1\,1\,0)} & (1 + \gamma_{1,1}(-\tau))\beta_k^{(0\,1\,1\,0)} \end{pmatrix} = \frac{1}{8}\begin{pmatrix} {}^{+}\alpha_{0,0}^{+} & {}^{-}\alpha_{0,0}^{+} \\ {}^{+}\alpha_{0,0}^{-} & {}^{-}\alpha_{0,0}^{-} \\ {}^{+}\alpha_{0,1}^{+} & {}^{-}\alpha_{0,1}^{+} \\ {}^{+}\alpha_{0,1}^{-} & {}^{-}\alpha_{0,1}^{-} \\ {}^{+}\alpha_{1,0}^{+} & {}^{-}\alpha_{1,0}^{+} \\ {}^{+}\alpha_{1,0}^{-} & {}^{-}\alpha_{1,0}^{-} \\ {}^{+}\alpha_{1,1}^{+} & {}^{-}\alpha_{1,1}^{+} \\ {}^{+}\alpha_{1,1}^{-} & {}^{-}\alpha_{1,1}^{-} \end{pmatrix}.$$

Proof. In order to determine the 16 coefficients ${}^{\pm}\alpha_{\xi_1,\xi_2}^{\sigma}$ in

$$\left(P\varphi_c^{\pm}\right)(k, x) = \sum_{\substack{\xi_1,\xi_2 \in \{0,1\} \\ \sigma \in \{+,-\}}} {}^{\pm}\alpha_{\xi_1,\xi_2}^{\sigma} \varphi_{\xi_1,\xi_2}^{\sigma}(k, x),\ x \in \mathbb{L}_T, \tag{16}$$

we first simplify the right-hand side by

$$\begin{aligned}\varphi^{\sigma}_{\xi_1,\xi_2}(k,x) &= \begin{pmatrix} e^{i\langle k+\xi_1\frac{b_1}{2}+\xi_2\frac{b_2}{2},x\rangle_2} \\ \sigma e^{i\langle k+\xi_1\frac{b_1}{2}+\xi_2\frac{b_2}{2},x+\tau\rangle_2}\end{pmatrix}\\ &= e^{i\langle \xi_1\frac{b_1}{2}+\xi_2\frac{b_2}{2},x\rangle_2}\begin{pmatrix} e^{i\langle k,x\rangle_2} \\ \sigma\gamma_{\xi_1,\xi_2}(\tau)e^{i\langle k,x+\tau\rangle_2}\end{pmatrix},\ \sigma\in\{+,-\}.\end{aligned}\tag{17}$$

For $x+\tau\in\mathbb{L}_T^{(\zeta_1,\zeta_2)},\ (\zeta_1,\zeta_2)\in\{0,1\}^2$ we further obtain due to $x=2j_1a_1+2j_2a_2$

$$e^{i\langle \xi_1\frac{b_1}{2}+\xi_2\frac{b_2}{2},x\rangle_2}=(-1)^{\zeta_1\xi_1+\zeta_2\xi_2}.$$

Now consider the left hand-side of (16) in terms of the splitting of $\mathbb{L}_T$, i.e.,

$$\left(P\varphi_c^{\pm}\right)(k,x),\ x+\tau\in\mathbb{L}_T^{(\zeta_1,\zeta_2)},\ (\zeta_1,\zeta_2)\in\{0,1\}^2.$$

For $x+\tau\in\mathbb{L}_T^{(0,0)}$ we have $x\in\mathbb{L}_G^{(1,1)}$ according to (11) (i.e., / in Figures 10 and 11). The application of the interpolation rule then yields,

$$\begin{aligned}\left(P\varphi_c^{\pm}\right)(k,x) &= \begin{pmatrix} w_s\left(e^{i\langle k,x+a_1-a_2\rangle_2}+e^{i\langle k,x-a_1+a_2\rangle_2}\right)\\ \pm\frac{1}{2}e^{i\langle k,x+\tau\rangle_2}\end{pmatrix}\\ &\quad+\begin{pmatrix} w_\ell\left(e^{i\langle k,x+a_1+a_2\rangle_2}+e^{i\langle k,x-a_1-a_2\rangle_2}\right)\\ \pm\frac{1}{2}e^{i\langle k,x+\tau\rangle_2}\end{pmatrix}\\ &= \begin{pmatrix} 2\left[w_s\cos(\langle k,a_1-a_2\rangle_2)+w_\ell\cos(\langle k,a_1+a_2\rangle_2)\right]e^{i\langle k,x\rangle_2}\\ \pm e^{i\langle k,x+\tau\rangle_2}\end{pmatrix}.\end{aligned}\tag{18}$$

For $x+\tau\in\mathbb{L}_T^{(0,1)}$ we have $x\in\mathbb{L}_G^{(1,0)}$ (/) and thus,

$$\begin{aligned}\left(P\varphi_c^{\pm}\right)(k,x) &= \begin{pmatrix} w_s\left(e^{i\langle k,x+a_1\rangle_2}+e^{i\langle k,x-a_1\rangle_2}\right)\\ \pm w_s\left(e^{i\langle k,x+\tau+a_2\rangle_2}+e^{i\langle k,x+\tau-a_2\rangle_2}\right)\end{pmatrix}\\ &\quad+\begin{pmatrix} w_\ell\left(e^{i\langle k,x+a_1-2a_2\rangle_2}+e^{i\langle k,x-a_1+2a_2\rangle_2}\right)\\ \pm w_\ell\left(e^{i\langle k,x+\tau+2a_1-a_2\rangle_2}+e^{i\langle k,x+\tau-2a_1+a_2\rangle_2}\right)\end{pmatrix}\\ &= \begin{pmatrix} 2\left[w_s\cos(\langle k,a_1\rangle_2)+w_\ell\cos(\langle k,a_1-2a_2\rangle_2)\right]e^{i\langle k,x\rangle_2}\\ \pm 2\left[w_s\cos(\langle k,a_2\rangle_2)+w_\ell\cos(\langle k,2a_1-a_2\rangle_2)\right]e^{i\langle k,x+\tau\rangle_2}\end{pmatrix}.\end{aligned}\tag{19}$$

Analogously we find for $x+\tau\in\mathbb{L}_T^{(0,1)}$ and $x\in\mathbb{L}_G^{(1,0)}$ (/),

$$\left(P\varphi_c^{\pm}\right)(k,x) = \begin{pmatrix} 2\left[w_s\cos(\langle k,a_2\rangle_2)+w_\ell\cos(\langle k,2a_1-a_2\rangle_2)\right]e^{i\langle k,x\rangle_2}\\ \pm 2\left[w_s\cos(\langle k,a_1\rangle_2)+w_\ell\cos(\langle k,a_1-2a_2\rangle_2)\right]e^{i\langle k,x+\tau\rangle_2}\end{pmatrix}.\tag{20}$$

Finally we obtain for $x+\tau\in\mathbb{L}_T^{(1,1)}$ and $x\in\mathbb{L}_G^{(0,0)}$ (/) that,

$$\left(P\varphi_c^{\pm}\right)(k,x) = \begin{pmatrix} e^{i\langle k,x\rangle_2}\\ \pm 2\left[w_s\cos(\langle k,a_1-a_2\rangle_2)+w_\ell\cos(\langle k,a_1+a_2\rangle_2)\right]e^{i\langle k,x+\tau\rangle_2}\end{pmatrix}.\tag{21}$$

Using the short-hand notation

$$\begin{aligned}\beta_k^{(0,0)}&=1,\\ \beta_k^{(0,1)}&=2\left[w_s\cos(\langle k,a_2\rangle_2)+w_\ell\cos(\langle k,2a_1-a_2\rangle_2)\right],\\ \beta_k^{(1,0)}&=2\left[w_s\cos(\langle k,a_1\rangle_2)+w_\ell\cos(\langle k,a_1-2a_2\rangle_2)\right],\\ \beta_k^{(1,1)}&=2\left[w_s\cos(\langle k,a_1-a_2\rangle_2)+w_\ell\cos(\langle k,a_1+a_2\rangle_2)\right],\end{aligned}$$

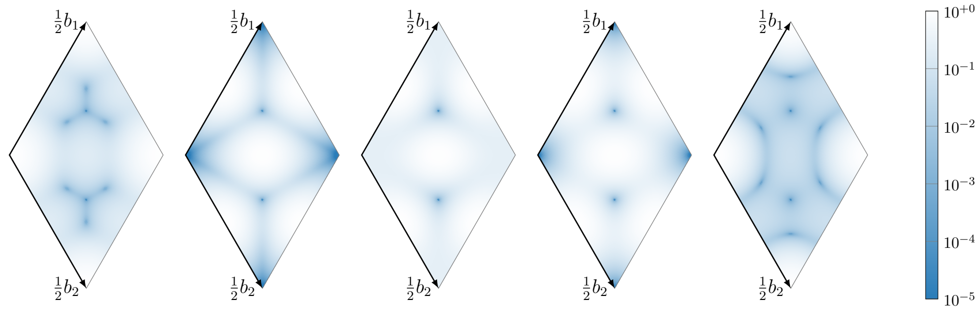

Figure 12: Logarithmic plots of the spectra of A_c for different choices of the long interpolation weight w_ℓ and $w_s = 2w_\ell - 1$ (from left to right: $w_\ell = 0$, $w_\ell = \frac{1}{6}$, $w_\ell = \frac{1}{4}$, $w_\ell = \frac{1}{3}$ and $w_\ell = \frac{1}{2}$).

we observe that $\beta_{\widehat{k}}^{(i_1\ i_2\ i_3\ i_4)}$ of (15) can be expressed by

$$\beta_k^{(i_1\ i_2\ i_3\ i_4)} = (-1)^{i_1}\beta_k^{(0,0)} + (-1)^{i_2}\beta_k^{(0,1)} + (-1)^{i_3}\beta_k^{(1,0)} + (-1)^{i_4}\beta_k^{(1,1)},$$

and obtain the following systems of equations by combining (18)–(21) with (17)

$$\begin{pmatrix} \beta_k^{(1-\zeta_1,1-\zeta_2)} \\ \pm\beta_k^{(\zeta_1,\zeta_2)} \end{pmatrix} = \sum_{\substack{\xi_1,\xi_2\in\{0,1\}\\ \sigma\in\{+,-\}}} \pm\alpha^\sigma_{\xi_1,\xi_2}(-1)^{\xi_1\zeta_1+\xi_2\zeta_2} \begin{pmatrix} 1 \\ \sigma\gamma_{\xi_1,\xi_2}(\tau) \end{pmatrix}, \quad \zeta_1,\zeta_2 \in \{0,1\}.$$

□

Lemma 15. *Given an interpolation operator P with interpolation weights w_s and w_ℓ, the Galerkin coarse grid operator $A_c = P^T AP$ on $\mathbb{L}_G^c$ for $A = A_{[0,-1]}$ on $\mathbb{L}_G$ is given by*

$$A_c = A_{[t_0,t_1,t_2,t_3,t_4]}$$

with $t_0 = t_2 = 0$ and

$$\begin{aligned} t_1 &= -6w_s^2 - 8w_s w_\ell - 2w_\ell^2 - 4w_s - 2w_\ell, \\ t_3 &= -4w_s w_\ell - 2w_s^2 - 2w_\ell^2 - 2w_\ell, \\ t_4 &= -2w_s w_\ell - 2w_\ell^2. \end{aligned}$$

Thus it can be represented by $A_{k,c}$ according to Lemma 11.

Corollary 16. *The coarse grid operator $A_c = P^T AP$ fulfills*

$$\dim(\mathrm{null}(A_c)) = \begin{cases} 4 & w_\ell \in (\frac{1}{6}, \frac{1}{3}), \\ 6 & w_\ell \in \{\frac{1}{6}, \frac{1}{3}\}, \\ 16 & \textit{else}, \end{cases}$$

where $w_s = 2w_\ell - 1$.

Proof. Using the result of Lemma 15 we find $A_c = A_{[t_1,t_2,t_3,t_4]}$. Generalizing Theorem 6 one finds again a 2×2 block-diagonalization of A_c and a description of its spectrum by $E_c(k)$. Using this representation we find[2] that for $w_\ell \in (\frac{1}{6}, \frac{1}{3})$ the

[2]Using a computer algebra system

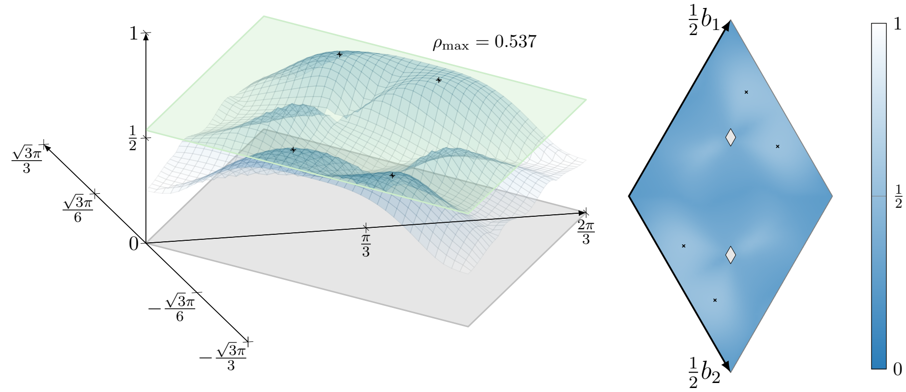

Figure 13: Amplification factors $\rho(M_k)$ of the two grid method for $k = k_1 b_1 + k_2 b_2$ with $(k_1, k_2) \in [0, \frac{1}{2})^2 \setminus \{(\frac{1}{6}, \frac{1}{3}), (\frac{1}{3}, \frac{1}{6})\}$ and $w_\ell = \frac{1}{4}$ (i.e., $w_s = -\frac{1}{2}$).

only doublet of zeros of $E_c(k)$ are located at the Dirac points. For $w_\ell \in \{\frac{1}{6}, \frac{1}{3}\}$ an additional doublet of zeros at $k = 0$ appears and for $w_\ell < \frac{1}{6}$ or $w_\ell > \frac{1}{3}$ there exists an $\alpha \in (0, 1)$ such that

$$\begin{aligned} E_c(\alpha K_1) &= 0, & E_c(\alpha K_2) &= 0, \\ E_c(b_1 + \alpha(K_1 - K_2)) &= 0, & E_c(b_2 - \alpha(K_1 - K_2)) &= 0, \\ E_c(b_1 + b_2 - \alpha K_1) &= 0, & E_c(b_1 + b_2 - \alpha K_2) &= 0. \end{aligned}$$

In Figure 12 the spectra of A_c on $\mathbb{D}_G$ for $w_\ell \in \{0, \frac{1}{6}, \frac{1}{4}, \frac{1}{3}, \frac{1}{2}\}$ are shown which illustrate all three cases. ∎

Now that all components of the two grid error propagator are analyzed we can formulate the main theorem.

Theorem 17. *Let $k = k_1 b_1 + k_2 b_2 \in \mathbb{D}_G$ with $k_1, k_2 \in [0, \frac{1}{2})$ the two grid operator M maps $H_k \to H_k$. Thus it can be represented by $M_k \in \mathbb{C}^{8 \times 8}$ with $M V_k = V_k M_k$ given by*

$$M_k = S_k \left(I - P_k A_{k,c}^{\dagger} P_k^T A_k \right) S_k,$$

where † denotes a suitable pseudo-inverse and P_k is defined by interpolation weights w_s and w_ℓ.

Proof. Follows directly from Lemmas 11 to 15. ∎

In Figure 13 the resulting amplification factors for the two grid operator with one pre- and one post-smoothing iteration are shown using $w_\ell = \frac{1}{4}$ (i.e., $w_s = -\frac{1}{2}$). The resulting largest amplification factor is approximately .55, i.e., the norm of an arbitrary error is at least almost halved in every iteration of the two grid method.

Based on Theorem 17 we show in Figure 14 the maximal amplification factors, i.e., convergence estimates, of the two grid method for varying interpolation weights w_ℓ. As already observed in Corollary 16 the existence of additional kernel modes for $w_\ell \notin (\frac{1}{6}, \frac{1}{3})$ leads to divergence. A stable plateau with an estimated convergence rate around .5 can be observed in the range $(\frac{1}{4}, \frac{1}{3} - \varepsilon)$. In contrast to $w_\ell \to \frac{1}{3}$ the method diverges already for w_ℓ significantly larger than $\frac{1}{6}$. This result proves the

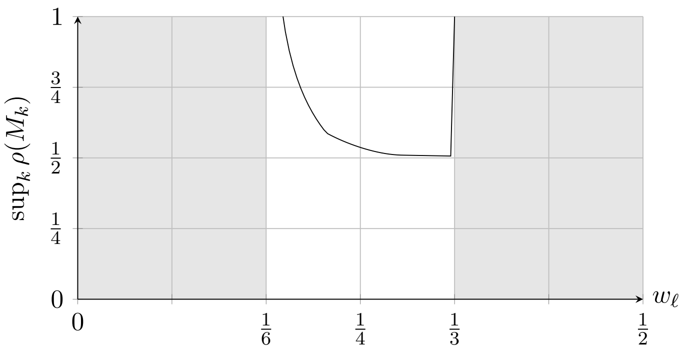

Figure 14: Plot of the estimated convergence rate of the two grid operator M using the interpolation weights w_ℓ and $w_s = 2w_\ell - 1$.

robustness and efficiency of the presented two-grid method to solve the maximally indefinite system arising in the tight-binding formulation of graphene.

5. Numerical results. In order to illustrate the findings in section 4 we consider a series of numerical tests. First, we show that asymptotically for $n, m, \ell \to \infty$ the theoretical bound is sharp for the range of interpolation weights, which was declared sensible. Second, we show that the performance of the method does neither depend on the aspect ratio of $\mathbb{G}_{n,m,\ell}$ nor on its chiral angle θ. We show that the recursive application of the construction yields a scalable multigrid method with convergence rate close to the two grid rate. Finally, we show results for non-periodic boundary conditions and discuss the difficulties that arise.

Two grid. We first consider the asymptotic convergence rate of the two grid method for varying interpolation weights $w_\ell \in (\frac{1}{6}, \frac{1}{3})$ and increasing lattice sizes $\mathbb{G}_{2^{k+1},2^{k+1},2^{k+1}}$ with periodic boundary conditions. As can be seen in Figure 15 the actual convergence rate stays strictly below the theoretical estimate for a wide range of interpolation weights. Towards the boundaries of $(\frac{1}{6}, \frac{1}{3})$ the behavior becomes erratic and divergence sets in earlier than predicted in the theory due to numerical instabilities. As expected the theoretical bound becomes sharper for increasing lattice sizes.

In a second set of tests we report in Figures 16 and 17 the behaviour of the two grid method with respect to changing aspect ratios and chiral angles of $\mathbb{G}_{n,m,\ell}$ by varying n, m and ℓ. In these tests the number of atoms is kept fixed at around 10^4. While the change in chiral angle at fixed aspect ratio has no influence on the two grid convergence (cf. Figure 17), the aspect ratio affects the asymptotic convergence rate (cf. Figure 16). This directly follows from Lemma 8, i.e., the change of the discrete spectrum $\Lambda_{n,m,\ell}$ with respect to n, m and ℓ.

Multigrid. Even though the developed theory only covers the two grid method, its construction is recursively applicable as the coarse grid operator is again formulated on a hexagonal lattice. In Figure 18 we report results of a multigrid V-cycle on $\mathbb{G}_{2^{k+1},2^{k+1},2^{k+1}}$ for varying interpolation weights $w_\ell \in (\frac{1}{6}, \frac{1}{3})$ using k levels in the multigrid hierarchy. The result shows that the theoretical two grid convergence estimate is not a sharp bound but still a good estimate for the k level multigrid V-cycle. The stagnation of the convergence rates for $k = 7$ and $k = 9$ indicate that the approach should scale well with increasing problem size and, concurrently, number of

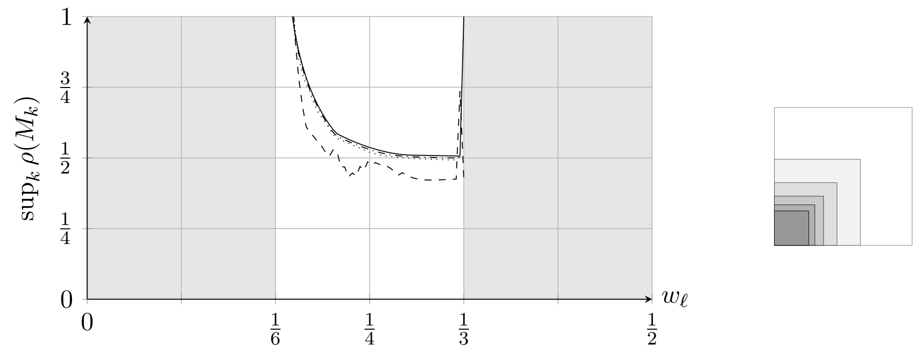

Figure 15: Theoretical bound of the convergence rate along with asymptotic convergence rates of the two grid method using the interpolation weights w_ℓ and $w_s = 2w_\ell - 1$ on lattices $\mathbb{G}_{2^{k+1},2^{k+1},2^{k+1}}$ (—— theor. bound, - - - - $k = 2$, ········ $k = 5$ and -·-·-· $k = 7$).

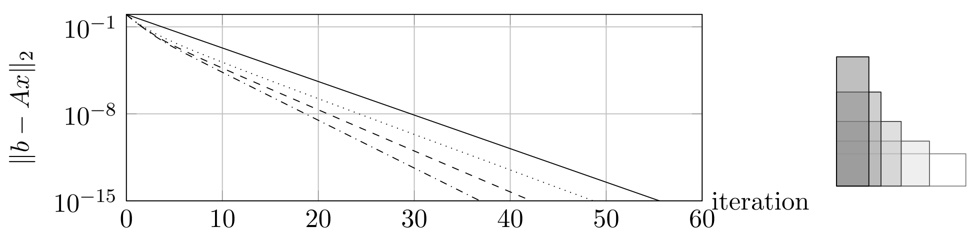

Figure 16: 16384 unknowns, aspect ratio $\alpha = \frac{\|C\|_2}{\|T\|_2}/\sqrt{3}$: (—— theor. bound, - - - - $\alpha = \frac{1}{16}$, ········ $\alpha = 1$ and -·-·-· $\alpha = 16$), Two-grid convergence using the interpolation weights $w_\ell = \frac{1}{4}$ and $w_s = -\frac{1}{2}$.

coarse grids.

Boundary conditions. Last, we consider graphene samples with open boundary conditions. As has been observed experimentally and shown analytically in [10] the presence of open boundary conditions along a zig-zag edge leads to localized eigenmodes along that edge which correspond to small eigenvalues. As can be seen in Figure 19 the presence of these eigenmodes stalls the convergence of our multigrid method. On the other hand, open boundary conditions along armchair boundaries do not hamper the scalability and convergence of the multigrid method. Note that already a single open zig-zag node, as present in the rotated samples, leads to localized eigenmodes. How to effectively treat these modes in the multigrid method remains an open question.

6. Conclusions. In this paper we have shown how to construct a scalable multigrid method with optimal complexity for the maximally indefinite system of equations arising in the tight-binding formulation of graphene. In addition we presented a rigorous convergence analysis of the two-grid scheme using LFA. The proven robustness with respect to size and shape of the graphene samples and the rapid convergence of the two-grid method transfers well to the multigrid method.

The efficient treatment of the local eigenmodes induced by open boundary condi-

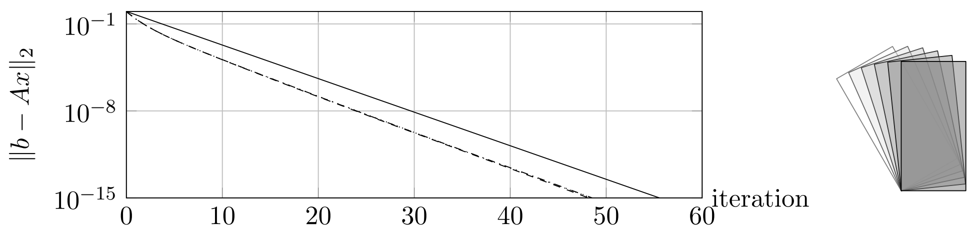

Figure 17: approx. $9k$ unknowns each, roughly the same aspect ratio $\frac{\|C\|_2}{\|T\|_2} \cdot \sqrt{3} \approx .4$, chiral angle θ (—— theor. bound, - - - - $\theta \approx 0°$, ········ $\theta \approx 7°$ and -·-·- $\theta \approx 21°$), Two-grid convergence using the interpolation weights $w_\ell = \frac{1}{4}$ and $w_s = -\frac{1}{2}$.

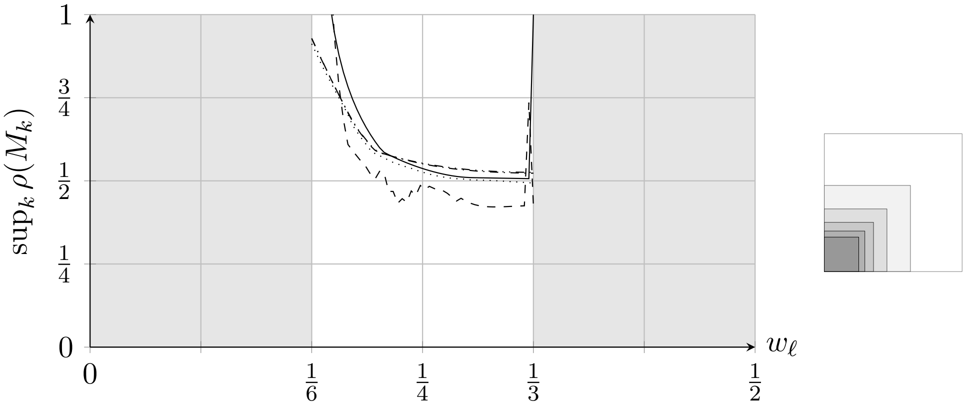

Figure 18: k-level Multigrid convergence. Lattice size $\mathbb{G}_{2^{k+1},2^{k+1},2^{k+1}}$ (—— theor. bound, - - - - $k = 2$, ········ $k = 5$, -·-·- $k = 7$ and -··-·· $k = 9$)

tions along zig-zag edges in the multigrid method remains an open question. We are currently in the process to incorporate our solver into the Monte-Carlo simulations for electronic-structure calculations described in [9, 22].

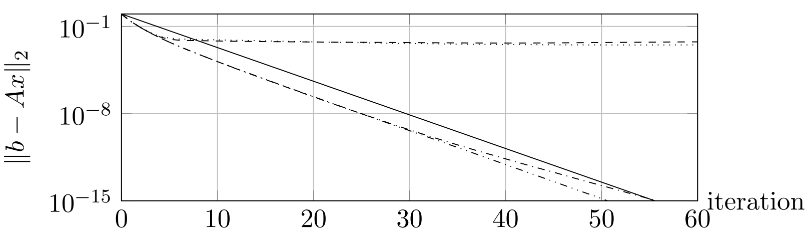

Figure 19: Convergence of the multigrid method ($w_\ell = \frac{1}{4}$ and $w_s = -\frac{1}{2}$, 5 level V-cycle) on $\mathbb{G}_{64,64,64}$ using different combinations of boundary conditions. In here (x_C,x_T) denotes the armchair b.c., x_C, and the zig-zag b.c., x_T, where p marks a periodic and o an open condition. —— theor. bound, - - - - (o, o), ········ (o, p), -·-·-· (p, o) and -···-··· (p, p).

References.

[1] R. E. Bank, *A comparison of two multilevel iterative methods for nonsymmetric and indefinite elliptic finite element equations*, SIAM J. Numer. Anal. 18.4 (1981), pp. 724–743, issn: 0036-1429, doi: 10.1137/0718048.

[2] A. Bayliss, C. I. Goldstein, and E. Turkel, *The numerical solution of the Helmholtz equation for wave propagation problems in underwater acoustics*, Comput. Math. Appl. 11.7-8 (1985), Computational ocean acoustics (New Haven, Conn., 1984), pp. 655–665, issn: 0898-1221, doi: 10.1016/0898-1221(85)90162-2.

[3] F. Bloch, *Über die Quantenmechanik der Elektronen in Kristallgittern*, Z. Phys. 52 (July 1929), pp. 555–600, doi: 10.1007/BF01339455.

[4] T. Boonen, J. V. Lent, and S. Vandewalle, *Local Fourier analysis of multigrid for the curl-curl equation*, SIAM J. Sci. Comput. 30.4 (Aug. 7, 2008), pp. 1730–1755, doi: 10.1137/070679119.

[5] J. H. Bramble, D. Y. Kwak, and J. E. Pasciak, *Uniform convergence of multigrid V-cycle iterations for indefinite and nonsymmetric problems*, SIAM J. Numer. Anal. 31.6 (1994), pp. 1746–1763, doi: 10.1137/0731089.

[6] J. H. Bramble, J. E. Pasciak, and J. Xu, *The analysis of multigrid algorithms for nonsymmetric and indefinite elliptic problems*, Math. Comp. 184 (1988), pp. 389–414, issn: 0025-5718, doi: 10.2307/2008755.

[7] A. Brandt, *Multi-level adaptive solutions to boundary-value problems*, Math. Comp. 31.138 (1977), pp. 333–390, doi: 10.2307/2006422.

[8] A. Brandt, *Rigorous quantitative analysis of multigrid, I. constant coefficients two-level cycle with L__2-norm*, SIAM J. Numer. Anal. 31.6 (1994), pp. 1695–1730, doi: 10.1137/0731087.

[9] P. V. Buividovich and M. I. Polikarpov, *Monte-Carlo study of the electron transport properties of monolayer graphene within the tight-binding model*, Phys. Rev. B 86 (Feb. 2012), p. 245117, doi: 10.1103/PhysRevB.86.245117.

[10] A. H. Castro Neto, F. Guinea, N. M. R. Peres, K. S. Novoselov, and A. K. Geim, *The electronic properties of graphene*, Rev. Mod. Phys. 81 (Jan. 2009), pp. 109–162, doi: 10.1103/RevModPhys.81.109.

[11] S. M.-M. Dubois, Z. Zanolli, X. Declerck, and J.-C. Charlier, *Electronic properties and quantum transport in graphene-based nanostructures*, Eur. Phys. J. B 72.1 (2009), p. 1, issn: 1434-6036, doi: 10.1140/epjb/e2009-00327-8.

[12] A. Frommer, K. Kahl, S. Krieg, B. Leder, and M. Rottmann, *Adaptive aggregation-based domain decomposition multigrid for the lattice Wilson–Dirac operator*, SIAM J. Sci. Comput. 36.4 (2014), A1581–A1608, doi: 10.1137/130919507.

[13] F. J. Gaspar, J. L. Gracia, and F. J. Lisbona, *Fourier analysis for multigrid methods on triangular grids*, SIAM J. Sci. Comput. 31.3 (2009), pp. 2081–2102, doi: 10.1137/080713483.

[14] A. Hirsch, *The era of carbon allotropes*, Nat. Mater. 9.11 (2010), pp. 868–871, doi: 10.1038/nmat2885.

[15] S. Kaczmarz, *Angenäherte Auflösung von Systemen linearer Gleichungen*, Bull. Pol. Acad. Sci. Math. 35 (1937), pp. 355–357.

[16] M. Lüscher, *Local coherence and deflation of the low quark modes in lattice QCD*, JHEP 07(2007)081 (2007), doi: 10.1088/1126-6708/2007/07/081.

[17] S. P. MacLachlan and C. W. Oosterlee, *Local Fourier analysis for multigrid with overlapping smoothers applied to systems of PDEs*, Numer. Linear Algebra Appl. 18.4 (2011), pp. 751–774, doi: 10.1002/nla.762.

[18] J. C. Osborn, R. Babich, J. Brannick, R. C. Brower, M. A. Clark, S. D. Cohen, and C. Rebbi, *Multigrid solver for clover fermions*, PoS LATTICE2010, 037 (2010).

[19] S. Reich, J. Maultzsch, C. Thomsen, and P. Ordejon, *Tight-binding description of graphene*, Phys. Rev. B 66.3 (2002), p. 035412, doi: 10.1103/PhysRevB.66.035412.

[20] Y. Shapira, *Multigrid techniques for highly indefinite equations*, in: *8th Copper Mountain Conference on Multigrid Methods*, 1995, pp. 689–705.

[21] U. Trottenberg, C. W. Oosterlee, and A. Schüller, *Multigrid*, vol. 33, Texts in Applied Mathematics. Bd. With contributions by A. Brandt, P. Oswald and K. Stüben, Academic Press, San Diego, 2001, isbn: 0-12-701070-X.

[22] M. Ulybyshev, P. Buividovich, M. Katsnelson, and M. Polikarpov, *Monte Carlo study of the semimetal-insulator phase transition in monolayer graphene with a realistic interelectron interaction potential*, Phys. Rev. Lett. 111.5 (2013), p. 056801, doi: 10.1103/PhysRevLett.111.056801.

[23] H. Yserentant, *On the multilevel splitting of finite element spaces for indefinite elliptic boundary value problems*, SIAM J. Numer. Anal. 23.3 (1986), pp. 581–595, issn: 0036-1429, doi: 10.1137/0723037.

[24] G. Zhou and S. R. Fulton, *Fourier analysis of multigrid methods on hexagonal grids*, SIAM J. Sci. Comput. 31.2 (2008/09), pp. 1518–1538, issn: 1064-8275, doi: 10.1137/070709566.